Dynamic Motion of Helix A in the Amino-Terminal Domain of Calmodulin Is Stabilized upon Calcium Activation†

Baowei Chen, M. Uljana Mayer, Lye Meng Markillie, David L. Stenoien, and Thomas C. Squier*

Cell Biology and Biochemistry Group, Biological Sciences Division, Fundamental Sciences Directorate, Pacific Northwest National Laboratory, P.O. Box 999, Richland, Washington 99352

Received August 3, 2004; Revised Manuscript Received October 26, 2004

ABSTRACT: Calcium-dependent changes in the internal dynamics and average structures of the opposing globular domains of calmodulin (CaM), as well as their relative spatial arrangement, contribute to the productive association between CaM and a range of different target proteins, affecting their functional activation. To identify dynamic structural changes involving individual α-helical elements and their modulation by calcium activation, we have used site-directed mutagenesis to engineer a tetracysteine binding motif within helix A near the amino terminus of calmodulin (CaM), permitting the selective and rigid attachment of the fluorescent probe 4′,5′-bis(1,3,2-dithioarsolan-2-yl)fluorescein (FlAsH) with full retention of function. The rigid tetracoordinate linkage of FlAsH to CaM, in conjunction with frequency domain fluorescence anisotropy measurements, allows assessment of dynamic changes associated with calcium activation without interference from independent probe motion. Taking advantage of the large fluorescence enhancement associated with binding of FlAsH to CaM, we determined rates of binding of FlAsH to apo-CaM and calcium-activated CaM to be 2800 ± 80 and 310 ± 10 M^{-1} s^{-1}, respectively. There is no difference in the solvent accessibility of the bound FlAsH irrespective of calcium binding to CaM. Thus, given that FlAsH selectively labels disordered structures, the large difference in rates of FlAsH binding indicates that calcium binding stabilizes helix A. Frequency domain anisotropy measurements of bound FlAsH indicate that prior to calcium activation, helix A undergoes large amplitude nanosecond motions. Following calcium activation, helix A becomes immobile, and structurally coupled to the overall rotation of CaM. We discuss these results in the context of a model that suggests stabilization of helix A relative to other domain elements in the CaM structure is critical to defining high-affinity binding clefts, and in promoting specific and ordered binding of the opposing lobes of CaM to target proteins.

Calmodulin (CaM)[1] is the primary intracellular calcium sensor in all eukaryotes. CaM regulates energy metabolism and diverse cellular processes underlying contraction, neurotransmission, and adaptive cellular responses through the rapid, calcium-dependent modulation of the function of more than 50 different target proteins, including kinases, phosphatases, ion channels, and pumps (*1*−*5*). Calcium ions bind to two EF-hand structures on each of the homologous domains; the four calcium binding sites are allosterically coupled through the central linker sequence (i.e., Met^{76} → Ser^{81}) connecting the opposing domains (Figure 1). Calcium binding is associated with domain activation and the exposure of hydrophobic sequences containing target protein binding sites with essentially no change in average secondary structure (*6*−*9*). Following calcium activation, CaM is able to bind to the wide range of target proteins through mechanisms that normally involve the initial association between the C-terminal domain of CaM and the CaM-binding

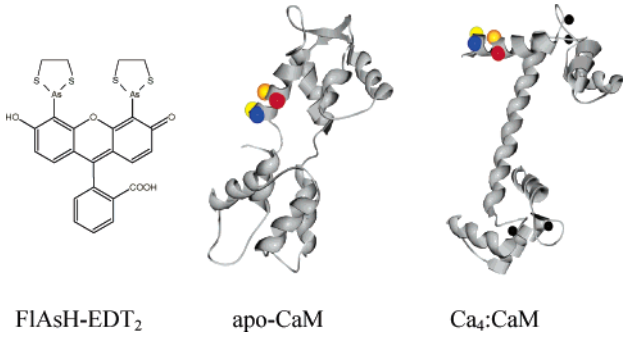

FIGURE 1: Depictions of structures for FlAsH-EDT_2, apo-CaM (PDB entry 1cfd), and calcium-saturated CaM (PDB entry 1cll). Secondary structural elements of CaM depict helices, sheets, loop structures, and when appropriate bound calcium (black spheres). Positions of mutated sites for FlAsH binding are highlighted in yellow, blue, gold, and red and correspond to cysteine substitutions at Glu^6, Glu^7, Ala^{10}, and Glu^{11}, respectively, in wild-type CaM.

† This work was supported by a grant from the National Institutes of Health (Grant AG17996) and by the U.S. Department of Energy, Office of Science Genomics: GTL project. Pacific Northwest National Laboratory is operated for the DOE by Battelle Memorial Institute under Contract DE-AC06-76RLO 1830.

* To whom correspondence should be addressed: Pacific Northwest National Laboratory, P.O. Box 999, Mail Stop P7-53, Richland, WA 99352. E-mail: thomas.squier@pnl.gov. Telephone: (509) 376-2218. Fax: (509) 372-1632.

[1] Abbreviations: CaM, calmodulin; EDTA, ethylenediaminetetraacetic acid; EGTA, ethylene glycol bis(β-aminoethyl ether)-*N*,*N*,*N*′,*N*′-tetraacetic acid; FlAsH-EDT_2, 4′,5′-bis(1,3,2-dithioarsolan-2-yl)-fluorescein (1,2-ethanedithiol)$_2$, also known as fluorescein arsenical helix binder; HEPES, *N*-(2-hydroxyethyl)piperazine-*N*′-2-ethanesulfonic acid; β-ME, 2-mercaptoethanol; NOE, nuclear Overhauser effect; SDS−PAGE, sodium dodecyl sulfate−polyacrylamide gel electrophoresis; TCEP, tris(carboxyethyl)phosphine.

10.1021/bi048332u CCC: $30.25
Published on Web 12/23/2004

sequence of the target protein, followed by the structural collapse and binding of the amino-terminal domain (*10*−*14*).

The fundamental mechanisms underlying the ability of CaM to selectively bind target proteins of variable structure with high affinity remain an area of active interest (*15*, *16*). Initial high-resolution structures of apo-CaM and calcium-activated CaM suggested the reorientation of individual helices upon calcium binding represents the critical switch that results in the exposure of the peptide binding clefts within each of the opposing domains of CaM (*17*−*19*). However, the recent availability of multiple high-resolution structures for both apo-CaM and calcium-activated CaM demonstrates the presence of considerable heterogeneity with respect to interhelical angles within each globular domain and in the structural linkage between the opposing domains of CaM (*7*, *20*−*22*). These latter results suggest that calcium-dependent changes in dynamic motions of structural elements within CaM may represent the primary switching mechanism for promoting binding to target proteins (*20*). Molecular dynamics (MD) simulations predict the presence of four subdomains within the amino-terminal lobe that have the potential to undergo large amplitude independent motions relative to one another (*23*). Indeed, helix A [$T^5 \rightarrow F^{19}$ (Figure 1)] is proposed to function as an independent subdomain that undergoes an independent motion with an amplitude of approximately 56° that is suggested to play a critical role in permitting the opposing domains of CaM to bind and activate a range of different target proteins of variable structure (*23*). In contrast, MD simulations indicate the carboxyl-terminal domain functions as a rigid structure that may facilitate binding to a specific site associated with the initial molecular recognition of target sequences (*23*).

To clarify the role of dynamic structural changes in the calcium activation of CaM, we have used site-directed mutagenesis to engineer a tetracysteine binding motif within helix A (Figure 1), permitting the selective and rigid attachment of the fluorescent probe 4′,5′-bis(1,3,2-dithioarsolan-2-yl)fluorescein (1,2-ethanedithiol)$_2$ (FLAsH-EDT$_2$) (*24*, *25*). Formation of the rigid tetracoordinate linkage of FlAsH to CaM induces a large increase in the quantum yield, ensuring an accurate measurement of the dynamics of helix A using frequency domain fluorescence spectroscopy without interference from independent probe motion. These measurements resolve calcium-induced changes in the structural interaction between helix A and the amino-terminal domain of CaM, and demonstrate that calcium activation induces a more rigid structure that can facilitate target protein binding. Likewise, calcium activation stabilizes the structural coupling between the opposing domains in CaM involving the central linker.

EXPERIMENTAL PROCEDURES

Materials. 4′,5′-Bis(1,3,2-dithoarsolan-2-yl)fluorescein (1,2-ethanedithiol)$_2$ (FLAsH-EDT$_2$) was synthesized as previously described (*24*, *25*). Adenosine deaminase and alkaline phosphatase were from Roche Diagnostics (Indianapolis, IN). Bovine heart cyclic nucleotide phosphodiesterase (PDE), *N*-(2-hydroxyethyl)piperazine-*N*′-(2-ethanesulfonic acid) (HEPES), tris(carboxyethyl)phosphine (TCEP), potassium iodide (KI), and cAMP were obtained from Sigma (St. Louis, MO). 2-Mercaptoethanol (β-ME) was obtained from Aldrich (Milwaukee, WI). Glycogen was obtained from ICN (Aurora, OH). All other chemicals were the purest grade commercially available.

Mutagenesis, Expression, and Purification of Cys^{6,7,10,11}-CaM. DNA encoding the tetracysteine mutant of calmodulin (Cys^{6,7,10,11}-CaM) was PCR amplified using the template containing wild-type CaM in a pBluescriptSKII vector (Stratagene, San Diego, CA). The forward primer (5′ CG GGG TAC CAT ↓ ATG GCT GAT CAA CTG ACA TGT TGT CAG ATT TGC TGT TTC AAA GA 3′) was designed to contain four mutagenic sites encoding cysteines (underlined) and a restriction site for NcoI (↓) to facilitate insertion of the CaM gene into a pET15b vector, while the T3 reverse primer (5′ AA TTA ACC CTC ACT AAA GGG 3′) defined the coding region for CaM. The 458 bp PCR-amplified product was digested with NcoI and BamHI, and was subsequently subcloned into a pET15b plasmid expression vector (Novagen, Madison, WI). Positive clones were screened and verified by DNA sequencing (Amplicon Express, Pullman, WA) and transformed into the BL21(DE3) *Escherichia coli* strain for protein expression. Following expression, mutant CaM was purified by chromatography on phenyl-Sepharose CL-4B (Pharmacia, Piscataway, NJ), essentially as previously described (*26*, *27*). The protein concentration of CaM was measured using a micro-BCA assay reagent kit (Pierce, Rockford, IL), using desalted CaM as a protein standard ($\epsilon_{277} = 3029\ M^{-1}\ cm^{-1}$) (*26*, *28*). Functional integrity of the mutant and labeled CaM was assessed through measurements of the CaM-dependent activation of PDE, as previously described (*29*).

Labeling with FlAsH-EDT$_2$. Prior to addition of 1.0 μM FlAsH-EDT$_2$, the CaM mutant (1.0 μM) containing the tetracysteine motif in helix A, where E6, E7, A10, and E11 were all mutated to cysteines (Figure 1), was incubated for 1 h at room temperature in 50 mM HEPES (pH 7.5), 140 mM NaCl, 1 mM β-ME, and 1 mM TCEP to reduce any disulfide bonds. Prior to fluorescence lifetime and anisotropy measurements, the mixture was incubated at 4 °C overnight.

Steady-State Fluorescence Measurements. Fluorescence emission spectra of the FlAsH−CaM species were measured with a Fluoro Max-2 fluorometer (SPEX, Edison, NJ), using excitation and emission slits of 5 nm. In all cases, the sample temperature was 25 °C, and the buffer consisted of 50 mM HEPES (pH 7.5), 140 mM NaCl, 1.0 mM β-ME, and 1.0 mM TCEP (buffer A) in the presence of either a calcium chelator (either 1.0 mM EDTA or EGTA) or saturating calcium concentrations (i.e., 0.2 mM $CaCl_2$). Changes in the solvent accessibility of FlAsH were assessed through collisional quenching, where variable amounts of a KI stock (4.0 M) were added to 1.0 μM FlAsH−CaM. Data were analyzed by measured changes in the fluorescence intensity, i.e., F_0/F, as a function of the titrated KI concentration and according to the Stern−Volmer equation:

$$F_0/F = 1 + K_{sv}[Q] = 1 + k_q\langle\tau\rangle[Q] \qquad (1)$$

where F_0 and F are the fluorescence intensity in the absence and presence of added KI, respectively, [Q] indicates the concentration of the quencher, KI, K_{sv} is the Stern−Volmer quenching constant, which is the product of both the average fluorescence lifetime in the absence of quencher ($\langle\tau\rangle$), and the bimolecular quenching constant (k_q) (*30*).

Frequency Domain Fluorescence. The fluorescence lifetime and anisotropy were measured using an ISS (Urbana, IL) K2 fluorometer, whose design has previously been described in detail elsewhere (*31*, *32*). Excitation utilized the 488 nm output from a Coherent (Santa Clara, CA) Innova 400 argon ion laser, and emitted light was collected after it had passed through a Schott OG-530 cutoff filter, using glycogen as a reference. All measurements were taken at 25 °C.

Analysis of Fluorescence Intensity and Anisotropy Decay. The frequency domain data were analyzed by a nonlinear least-squares method (*33*, *34*). The time-dependent decay $I(t)$ of fluorescence is generally fit to a sum of exponentials:

$$I(t) = \sum_{i=1}^{n} \alpha_i e^{-t/\tau_i} \quad (2)$$

where α_i values represent the pre-exponential factors, τ_i values represent the decay times, and n is the number of exponential components required to describe the decay. The intensity decay law is obtained from the frequency response of amplitude-modulated light and is characterized by the frequency-dependent values of the phase and the extent of demodulation. The values are compared with the calculated values from an assumed decay law until a minimum of the squared deviation (χ_R^2) is obtained. After the measurement of the intensity decay, the average lifetime was calculated:

$$\langle \tau \rangle = \frac{\sum_{i=1}^{n} \alpha_i \tau_i^2}{\sum_{i=1}^{n} \alpha_i \tau_i} = \sum_{i=1}^{n} f_i \tau_i \quad (3)$$

where f_i values represent the fractional intensities associated with each of the pre-exponential terms and $\langle \tau \rangle$ is directly related to the average time during which the fluorophore is in the excited state.

The frequency domain anisotropy decays $r(t)$ were fit to a multiexponential model:

$$r(t) = r_0 \sum_{i=1}^{n} g_i e^{-t/\phi_i} \quad (4)$$

where r_0 is the limiting anisotropy in the absence of rotational diffusion, φ_i values are the rotational correlation times, g_i represents the amplitude of the total anisotropy loss associated with each rotational correlation time, and n is the total number of components associated with the fluorescence decay (*35*). In all cases, parameter values are determined by minimizing the χ_R^2, which serves as a goodness-of-fit parameter that provides a quantitative comparison of the deviations between the measured and calculated values. Errors in the differential phase and modulated anisotropy were assumed to be 0.2° and 0.005, respectively.

RESULTS

Construction and Chemical Modification of a CaM Mutant for Fluorescence Measurements. Using site-directed mutagenesis, we have introduced a tetracysteine motif into helix A of CaM, permitting the covalent attachment of the biarsenical compound FlAsH (*24*) (Figure 1). Modified residues are solvent exposed in the crystal structures, and are not involved in any proposed contact interactions between either Ala[1], Asp[2], and Leu[4] near the amino terminus or Gln[8] and Phe[12] in helix A and Met[76], Lys[77], and Asp[80] in the central linker of CaM (*36*). The specificity of FlAsH for tetracysteine CaM is highlighted by cellular labeling of the tetracysteine-CaM mutant expressed in *E. coli*. *In vivo* CaM labeling by FlAsH was assessed following expression of the tetracysteine CaM mutant using intact *E. coli*, permitting a rapid determination of the potential of FlAsH to selectively label proteins of interest. Following incubation with FlAsH, one observes that cells expressing CaM are selectively labeled (Figure 2A). There is heterogeneity in cellular labeling, which is related to inefficiencies in the partitioning of the FlAsH label into *E. coli* that result in fluorescent labeling of less than 10% of the *E. coli* cells (data not shown).

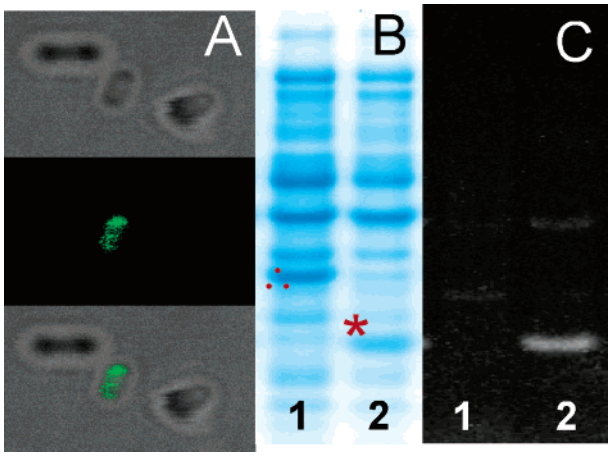

FIGURE 2: Specificity of CaM labeling with FlAsH-EDT_2. The specificity of the FlAsH-EDT_2 for the tetracysteine motif on CaM was assessed following induction of CaM expression in *E. coli* cells. (A) Confocal images obtained from a Leica TCSP2 spectral confocal laser scanning microscope following application of 0.6 μM FlAsH reagent showing a phase contrast image (top), fluorescence (middle), and superposition of two images (bottom). (B and C) Following cell disruption and separation by SDS−PAGE, cellular proteins were imaged following Coomassie brilliant blue staining (B) or detection of fluorescence following excitation of FlAsH-labeled proteins (C). Shown are lysates from *E. coli* expressing cytochrome c_3 (lane 1, dotted triangle) or the tetracysteine-containing CaM mutant (lane 2, asterisk). Fluorescence intensity associated with both CaM and its dimer is apparent in lane 2.

For comparison purposes, a control sample was examined that overexpresses cytochrome c_3, which does not contain a tetracysteine labeling site (left lanes, Figure 2). The specificity of CaM labeling was determined following cellular disruption and separation of expressed proteins using SDS−PAGE. The total protein was stained using Coomassie brilliant blue (Figure 2B), and FlAsH-tagged proteins were imaged under ultraviolet light (Figure 2C). It is apparent that CaM containing the tetracysteine sequence in helix A is selectively labeled with FlAsH with minimal background fluorescence. In contrast, there was no significant labeling of any protein in the control sample (left lane, Figure 2C). These results provide strong evidence that biarsenical affinity reagents selectively target the tetracysteine motif on CaM.

Retention of CaM Function following Site-Directed Mutagenesis and FlAsH Binding. The tetracysteine tag engi-

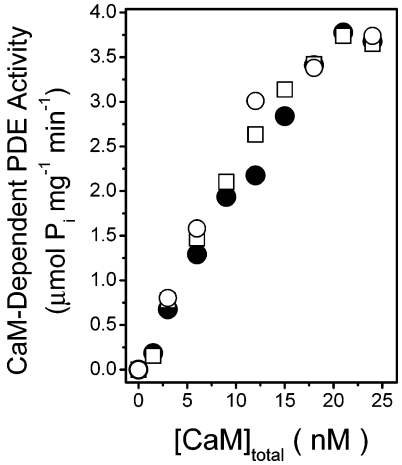

FIGURE 3: Function of the CaM mutant. The CaM dependence of the activation of cyclic nucleotide phosphodiesterase was measured using either wild-type CaM (○) or mutant CaM containing the tetracysteine motif in helix A before (●) and following (□) label incorporation. The assay involved measurement of the CaM-dependent activity of 0.003 unit of PDE/mL in 100 mM glycylglycine (pH 7.5), 2.1 mM $CaCl_2$, 40 mM $MgSO_4$, and 2.9 mM cAMP in the presence of 30 units/mL alkaline phosphatase and 4 units/mL adenosine deaminase, essentially as previously described (*29*). The CaM-indepenent activity of PDE was 0.7 μmol of P_i mg^{-1} min^{-1}.

neered into helix A faces away from other structural elements (Figure 1); modification of this site with FlAsH is therefore not expected to affect the structure of CaM (*24*). Additional resolution of possible structural perturbations was determined from a consideration of the CaM-dependent activation of phosphodiesterase (PDE), which has previously been used to infer possible structural perturbations resulting from site-directed mutagenesis (*37*). The mutant and fluorescently labeled CaM retains the ability to fully activate phosphodiesterase, with essentially no change in either the apparent affinity or maximal extent of enzyme activation (Figure 3). Thus, the FlAsH-labeled CaM is expected to accurately report calcium-dependent changes in the dynamics of helix A and its structural coupling with the amino- and carboxyl-terminal domains of CaM that can be measured using frequency domain fluorescence spectroscopy (see below).

Conformation-Specific Labeling of CaM. FlAsH-EDT_2 binds to the tetracysteine motif in helix A to become highly fluorescent. Under conditions in which CaM is in large molar excess relative to FlAsH-EDT_2, there is a linear relationship between the pseudo-first-order rate constant associated with FlAsH binding and the concentration of CaM that is indicative of a reaction mechanism involving second-order kinetics (data not shown). Using the same molar stoichiometries of FlAsH-EDT_2 and CaM, large differences are observed in the kinetics of *in vitro* FlAsH labeling for apo-CaM and calcium-activated CaM. The rate of labeling decreases from 2800 ± 80 M^{-1} s^{-1} for apo-CaM to 310 ± 10 M^{-1} s^{-1} for calcium-activated CaM (Figure 4A). The 89 ± 1% decrease in the rate of labeling following calcium activation of CaM indicates that there are substantial differences in the conformation of helix A in apo-CaM and calcium-activated CaM, since FlAsH has previously been demonstrated to selectively bind to conformationally disordered sequences (*25*). The observed structural differences do not significantly affect the environment around FlAsH, as evidenced by the fluorescence emission spectra, which

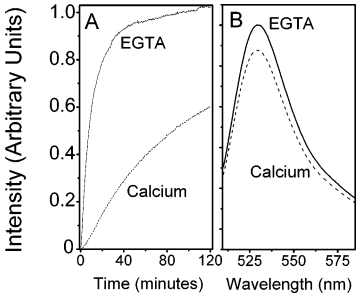

FIGURE 4: FlAsH labeling of apo-CaM and calcium-saturated CaM. (A) The kinetics of FlAsH binding to apo-CaM or Ca_4-CaM was followed by the resulting fluorescence enhancement following addition of 1.0 μM FlAsH-EDT_2. (B) Calcium-dependent changes in fluorescence emission spectra of FlAsH bound to CaM. Experimental conditions involved 1.0 μM CaM in buffer A [50 mM HEPES (pH 7.5), 140 mM NaCl, 1 mM β-ME, and 1 mM TCEP] in the presence of 1 mM EDTA (—) or 0.2 mM $CaCl_2$ (- - -) at 25 °C. Excitation was at 500 nm, and fluorescence emission was measured at 530 nm. Rate constants were calculated from the data in panel A, taking into account that the concentrations of reactants (i.e., FlAsH-EDT_2 and CaM) are identical at time zero. Under these conditions, the general rate law simplifies to $1/[\text{FlAsH}\cdot\text{EDT}_2]_t - 1/[\text{FlAsH}\cdot\text{EDT}_2]_0 = kt$, where $[\text{FlAsH}\cdot\text{EDT}_2]_0$ and $[\text{FlAsH}\cdot\text{EDT}_2]_t$ are the initial and remaining concentrations of FlAsH·EDT_2, respectively (*65*).

are very similar for apo-CaM and calcium-activated CaM, exhibiting the same emission maximum near 530 nm (Figure 4B). Calcium binding results in a 12−13% decrease in fluorescence intensity; the minimal sensitivity of FlAsH to calcium binding is consistent with the reported insensitivity of the quantum yield of this probe to protein conformation and permits its facile use in measuring protein dynamics (*38*). Since the large increase in the quantum yield of FlAsH requires binding to all four cysteines (*25*), all fluorescent probes are rigidly bound and report the dynamics of the helix A backbone.

Calcium-Dependent Change in the Conformation of Helix A. Additional resolution of calcium-induced conformational changes associated with helix A is possible from a consideration of the time-dependent fluorescence decays, which are particularly sensitive to the environment around the fluorophore (*30*, *39*, *40*). We have used frequency domain fluorescence spectroscopy to measure the time-dependent decays of FlAsH bound to CaM. In these measurements, the frequency of the incident light is sinusoidally modulated; following emission from the FlAsH-labeled CaM, the phase is shifted to longer times and the depth of the modulated light is diminished relative to the excitation. The extent of the phase shift and modulation decrease are inversely related to the lifetime of the fluorophore, where a shift in the frequency response to higher frequencies is indicative of a shorter average excited-state lifetime. A shorter excited-state lifetime, in turn, is a general indicator of increased polarity due to either greater solvent exposure or the increased proximity of polar or charged side chain moieties.

Upon increasing the modulation frequency, one observes a progressive increase in the phase lag and a decrease in the amplitude of the modulation relative to the incident light (Figure 5). In comparison to apo-CaM, there is a shift in the frequency response of calcium-activated CaM toward higher frequencies, indicative of a calcium-dependent decrease in the average lifetime that is consistent with the steady-state fluorescence measurements (Figure 4). In all cases, nonlinear

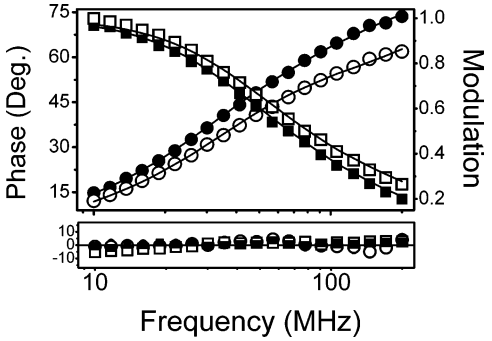

FIGURE 5: Lifetime-resolved fluorescence intensity decays for FlAsH-bound CaM. The frequency response and associated nonlinear least-squares fits to a two-exponential decay for the phase shift (● and ○) and modulation (■ and □) for FlAsH covalently bound to helix A for apo-CaM (● and ■) and calcium-saturated CaM (○ and □). Weighted residuals (shown below the data) correspond to the difference between the experimental data and the calculated fit divided by the standard error of the individual measurement, assumed to be 0.2° and 0.005 for phase and modulation data, respectively. Experimental conditions involved 1.0 μM CaM in buffer A in the presence of either 1.0 mM EGTA or 0.2 mM $CaCl_2$ at 25 °C.

least-squares fits to the data can be described by a sum of two exponentials, as indicated by the random distribution of the weighted residuals (Table 1). In comparison to apo-CaM, there is a 17 ± 3% decrease in the average lifetime of the fluorophore in the calcium-bound state that is reflected in decreases in each of the individual lifetime components (τ_i); however, significant differences are observed in the contributing amplitudes (α_i) that are indicative of changes in the environments around FlAsH in apo-CaM and calcium-activated CaM.

Helix A Remains Solvent Accessible following Calcium Activation of CaM. Possible causes underlying the observed differences in the fluorescence lifetime decay of FlAsH bound to apo-CaM and calcium-activated CaM may be the result of global changes in the tertiary structure of CaM that alter the environment around the fluorophore. Therefore, to distinguish between changes in the structure of helix A from global tertiary structural changes that alter contact interactions between the FlAsH label and other structural elements of CaM, we have measured the solvent accessibility of FlAsH using iodide as a collisional quencher. Changes in the fluorescence intensity (F_o/F) as a function of quencher concentration multiplied by the average fluorescence lifetime (i.e., $\langle\tau\rangle$) directly take into account ligand-dependent changes in the average lifetime of FlAsH (see eq 1 in Experimental Procedures). Upon increasing the concentration of KI, one observes a progressive decrease in fluorescence intensity (i.e., F_o/F increases) that is virtually identical for apo-CaM and calcium-activated CaM (Figure 6 and Table 1). Thus, observed alterations in the environment around the FlAsH label associated with the calcium activation of CaM are the result of dynamic changes in helix A, as there are no changes in tertiary contact interactions between this face of helix A and other structural elements in CaM that would sterically affect the solvent accessibility of FlAsH bound to helix A.

Dynamic Stabilization of Helix A following Calcium Activation. Dynamic structural changes associated with helix A were measured using frequency domain fluorescence anisotropy, permitting resolution of independent helix motions from the overall rotational dynamics of the entire CaM protein (*41*). The differential phase and modulated anisotropy of FlAsH bound to apo-CaM and calcium-activated CaM were collected over 20 frequencies between 10 and 200 MHz (Figure 7), permitting a determination of both the rates and amplitudes of helix A motion. In these measurements, the modulation frequency is directly related to the rate of motion such that high and low frequencies correspond to fast and slow rates of motion, respectively. Furthermore, the modulated anisotropy observed after long times (i.e., 10 MHz) is a reflection of the residual anisotropy that is related to the amplitude of helix A motion, while that observed after short times (i.e., 200 MHz) provides an indication of the initial anisotropy that is related to the extent of the fluorescence anisotropy decay that is resolved (*30*). Likewise, faster rates of motion result in larger changes in the differential phase at lower modulation frequencies.

The modulated anisotropy at 200 MHz is 0.31 for both apo-CaM and calcium-activated CaM, which is close to the theoretical maximum of 0.4, indicating that we have resolved the majority of the fluorescence anisotropy decay, and that FlAsH is rigidly bound to the tetracysteine motif in helix A. One observes that for apo-CaM, the differential phase increases from 3° at 10 MHz to a maximum of approximately 8° at 60 MHz (Figure 7A). In contrast, a much smaller change in the differential phase is observed following calcium activation, which increases from 2° at 10 MHz to a maximum of 4.6° at 50 MHz. Likewise, there are significant differences in the residual anisotropy at 10 MHz, which increases from 0.24 for apo-CaM to 0.26 following calcium activation. These results indicate that helix A experiences a decreased rate and amplitude of motion upon calcium activation.

A nonlinear least-squares fit of the data to determine the rates and amplitudes of motion provides a quantitative understanding of the underlying causes of the change in the fluorescence anisotropy data. The fluorescence anisotropy decays for apo-CaM require two rates of motion to adequately describe the data, corresponding to the motion of helix A (φ_1 = 1.1 ± 0.5 ns) and a longer rotational correlation time associated with the hydrodynamic properties of the amino-terminal domain (φ_2 = 10 ± 1 ns) (Table 2). In contrast, a single rotational correlation time fully describes the anisotropy decay for calcium-activated CaM (φ_2 = 15 ± 2 ns) (Table 2), as judged by the randomly weighted residuals (Figure 7C, D). The observed rotational correlation time agrees with hydrodynamic calculations for the overall rotational dynamics of calcium-activated CaM using the structure in Figure 1 (i.e., $\varphi_r = 1/6D_r$ = 15.7 ns), suggesting that this structure approximates the major conformer in solution (*42*, *43*). These measurements are in agreement with prior results using fluorescent probes at multiple locations in the amino- and carboxyl-terminal lobes of calcium-activated CaM, as well as recent NMR measurements (*44*−*47*). Thus, following calcium activation, helix A becomes structurally coupled to the entire CaM molecule.

The longer rotational correlation time for apo-CaM, corresponding to motion of the amino-terminal domain, is significantly shorter than that associated with the overall rotational dynamics of calcium-activated CaM, as judged by the lack of overlap in the error surfaces in a rigorous analysis of correlated errors in the fit to the data (*48*) (Figure 8). The amplitude associated with the independent motion of helix A [i.e., g_1 = 0.10 ± 0.04 (Table 2)] permits the calculation

Table 1: Lifetime Data and Solvent Accessibility for FlAsH-Labeled CaM[a]

ligand	α_1	τ_1 (ns)	α_2	τ_2 (ns)	$\langle\tau\rangle$[b] (ns)	k_q[c] ($\times 10^{-8}$ M^{-1} s^{-1})
EGTA	0.34 ± 0.01	1.2 ± 0.2	0.66 ± 0.01	4.5 ± 0.1	4.1 ± 0.1	2.4 ± 0.2
Ca^{2+}	0.52 ± 0.02	0.80 ± 0.09	0.48 ± 0.02	4.0 ± 0.1	3.4 ± 0.1	2.2 ± 0.1

[a] Average amplitudes (α_i) and lifetimes (τ_i) obtained from two-exponential fits to frequency domain data for the time-dependent intensity decay, $I(t)$, for FlAsH covalently bound to Cys^6, Cys^7, Cys^{10}, and Cys^{11} engineered into helix A of CaM, assuming $I(t) = \sum_i \alpha_i \exp(-t/\tau_i)$. [b] $\langle\tau\rangle = \sum_i \alpha_i \tau_i^2 / \sum_i \alpha_i \tau_i$. Errors represent the standard errors of the mean for three independent measurements. [c] Bimolecular quenching constant determined from the slope in Figure 6. Experimental conditions include 1.0 μM FlAsH-bound CaM in 50 mM HEPES (pH 7.5), 140 mM NaCl, 1.0 mM β-mercaptoethanol, 1.0 mM TCEP, and either 1.0 mM EGTA (EGTA) or 0.2 mM $CaCl_2$ (Ca^{2+}) at 25 °C.

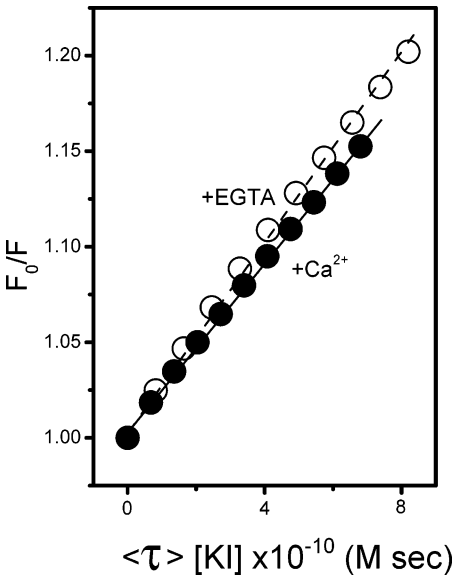

FIGURE 6: Solvent accessibilities of FlAsH-bound CaM. Modified Stern−Volmer plots of the quenching of FlAsH bound to CaM for apo-CaM (○) and calcium-saturated CaM (●) for 1.0 μM FlAsH-labeled CaM in buffer A in the presence of either 1.0 mM EGTA (○) or 0.2 mM $CaCl_2$ (●). Fluorescence quenching data (i.e., F_o/F) were plotted against the product of the average lifetime and the quencher concentration ($\langle\tau\rangle$[KI]), where the slope is a direct measure of the bimolecular quenching constant (k_q). $\lambda_{ex} = 500$ nm; $\lambda_{em} = 530$ nm.

of the amplitude of motion, which corresponds to a full cone angle of $30 \pm 6°$ (Figure 9) (*49*−*51*). This latter result is consistent with previously published NMR data, which observed strong interhelical NOE interactions involving the tips of EF-hand helices only for apo-CaM, suggesting a scissor-type motion involving interhelical angles whose full amplitude of motion corresponds to more than 25° (*7*). Taken together, these results indicate considerable dynamic flexibility for helix A, and by implication the amino-terminal domain, in apo-CaM. Following calcium activation, the dynamic structure of the amino-terminal domain is stabilized, and the amino- and carboxyl-terminal domains become conformationally coupled (Figure 9).

DISCUSSION

Summary of Results. We have engineered a fully functional CaM mutant in which the site-directed substitution of four cysteines into helix A has permitted the investigation of calcium-dependent changes in the conformational dynamics and structural coupling between the FlAsH fluorophore rigidly bound to helix A and the amino- and carboxyl-terminal globular domains of CaM. There is no difference in the solvent accessibility of FlAsH bound to apo-CaM and calcium-activated CaM (Figure 6), indicating that the $89 \pm 1\%$ decrease in the rate of FlAsH labeling following calcium activation of CaM is unrelated to any steric effects due to changes in the tertiary structure of CaM. Rather, the decreased rate of labeling is the result of the selectivity of FlAsH binding to sequences with greater conformational disorder (*25*). These results indicate a large increase in the stability of helix A when CaM is in the calcium-bound state (Figure 4). Likewise, large amplitude motions of helix A occur in apo-CaM; following calcium binding, helix A becomes structurally coupled to the entire CaM molecule (Figure 9 and Table 2). The slower labeling kinetics and observed structural linkage between helix A and the remainder of the protein are consistent with reported contact interactions between helix A and the central linker sequence (i.e., Arg^{76}−Ser^{81}) that modulate the stability and calcium affinity of the amino-terminal domain (*36*). Thus, stabilization of an activated conformation of the amino-terminal domain following calcium binding predisposes CaM to binding with high affinity to a range of target proteins with nonhomologous sequences. The proposed structural linkage between helix A and the opposing carboxyl-terminal globular domain through the central linker sequence is, furthermore, consistent with previous measurements that have also implicated structural and functional linkages between the central sequence and the opposing globular domains of CaM (*3*, *21*, *27*, *36*, *52*−*60*). Together, these results suggest a critical role for helix A, which functions as part of a conformational switch in modulating calcium-induced interdomain interactions, and the activated conformation of CaM associated with the calcium-dependent binding and activation of target proteins.

Molecular Dynamics Simulations. High-resolution structures of CaM suggest an important role for rigid body helical motions and the internal dynamics of CaM in mediating the wide range of binding interactions associated with target protein activation and signal transduction (*20*). Insight into the possible roles of helix A and protein dynamics in the modulation of CaM function is available from numerous molecular dynamics simulations, which provide predictions regarding possible CaM domain motions and suggest a critical role for changes in these dynamics in the modulation of binding of CaM to target proteins (*9*). Calcium binding induces a mechanical force that shortens the distances between the ends of the helices to alter the interhelical angles within individual EF-hands (*8*). Prior to calcium binding, large amplitude helical motions are believed to occlude the peptide binding site on the amino-terminal domain of CaM; calcium activation is thought to stabilize a more open and less dynamic structure that favors binding to target proteins (*61*). These motions within the amino-terminal domain of CaM are suggested to occur on the nanosecond time scale

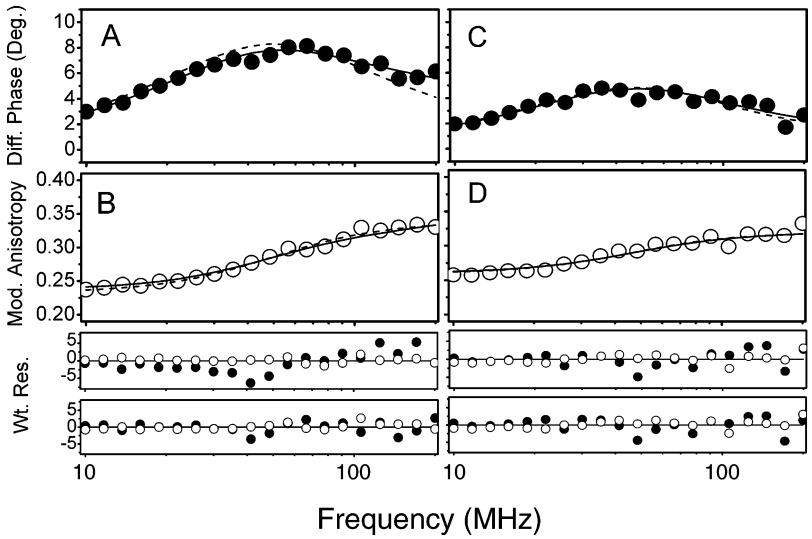

FIGURE 7: Calcium-dependent change in the rotational dynamics of FlAsH-labeled CaM. Differential phase angles (●) and modulated anisotropies (○) were measured for 1.0 μM FlAsH-bound CaM in buffer A in the presence of either 1.0 mM EGTA (left panels) or 0.2 mM $CaCl_2$ (right panels). Nonlinear least-squares fits are illustrated for models corresponding to a single rotational rate (- - -) or two rotational rates (—). Weighted residuals (Wt. Res.) corresponding to the experimental data minus the calculated value normalized by the standard errors for the measurements are illustrated for the single-exponential (top) and two-exponential (bottom) models. Errors in the measurement of the differential phase and modulated anisotropy were assumed to be 0.2° and 0.005, respectively.

Table 2: Rotational Dynamics of FlAsH-Bound CaM[a]

ligand	g_1	φ_1 (ns)	g_2	φ_2 (ns)	χ_R^2
EGTA	0.10 ± 0.04	1.1 ± 0.5	0.90 ± 0.03	10 ± 1	4.3
Ca^{2+}	—	—	1.0	15 ± 2	5.1

[a] Indicated values are for the pre-exponential terms (i.e., g_i) and rotational correlation times (i.e., φ_i) with associated standard errors of the mean obtained from three independent measurements of the anisotropy decay, $r(t)$, which equals $r_o\sum_i g_i \exp(-t/\varphi_i)$. The limiting anisotropy (i.e., r_0) was 0.34 ± 0.04. The goodness of fit (i.e., χ_R^2) was calculated assuming frequency-independent errors in the differential phase and modulated anisotropy, which were assumed to be 0.2° and 0.005, respectively. Experimental conditions are as described in the legend of Figure 7.

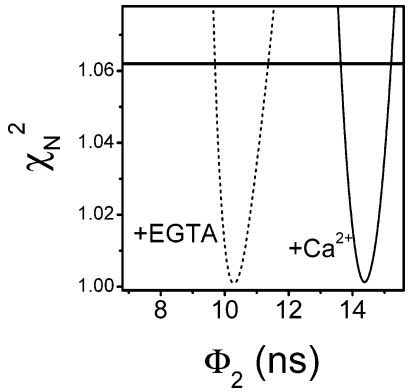

FIGURE 8: Depiction of error surfaces for overall rotational dynamics of CaM. Parameter values were obtained from a simultaneous fit to three data sets to rigorously assess the errors associated with the determination of overall rates of rotational motion for apo-CaM (⋯) and calcium-activated CaM (—). Experimental values for the overall rate of rotational motion (i.e., φ_2) were incrementally adjusted, and all other parameters were allowed to vary in the least-squares analysis, essentially as previously described (*46*, *48*). The resulting goodness of fit was normalized to the optimal value (χ_N^2), where the standard deviation was determined to fall within χ_N^2 values of <1.062 (solid horizontal line), which corresponds to the *F* statistic. Experimental conditions are as described in the legend of Figure 7. Expected values for the overall rotational correlation times ($1/6D_r$) for the motion of the entire protein were calculated to be 14.5 ns for apo-CaM and 15.7 ns for calcium-saturated CaM from the crystal structures (see Figure 1), assuming rigid coupling between the opposing domains (*43*).

(*23*), consistent with the large amplitude motions of helix A observed in apo-CaM (Table 2 and Figure 9). Indeed, these prior MD simulations indicate that the amino-terminal lobe of CaM splits into four subdomains that undergo concerted motions, while the carboxyl-terminal domain comprises a single rigid domain. Furthermore, the 11 amino acids in helix A are suggested to form an independent subdomain, which undergoes substantial angular displacements (i.e., ~56°) during the time course of the simulation (*23*). Our results indicate the formation of a structural linkage between helix A, the rest of the amino-terminal domain, and the carboxyl-terminal domain of CaM following calcium activation (Figures 7 and 8 and Table 2). These results are, furthermore, consistent with prior suggestions that interactions between amino acids within helix A and the central linker of CaM modulate the dynamics and calcium affinity within the amino-terminal domain of CaM (*36*, *59*). Further, the structural linkage between helix A and the central sequence [i.e., helices D and E (Figure 9)] suggests a mechanistic basis for observed allosteric interactions between calcium binding sites in the carboxyl- and amino-terminal domains of CaM (*36*, *45*, *52*, *58*).

Dynamical Structure of CaM. The role of the central sequence in mediating allosteric coupling between the opposing domains has been controversial. For example, Bax and co-workers have suggested that the opposing domains of CaM are structurally uncoupled at acidic pH, with calcium activation resulting in a reduction in the helical content of the central sequence (*7*, *19*, *62*). However, considerable heterogeneity is apparent in the multiple high-resolution structures of both apo-CaM and calcium-activated CaM. This heterogeneity is represented by differences in the interhelical angles, in the secondary structures of the central linker, and in the corresponding spatial arrangements of the opposing domains (*7*, *17*—*22*). Indeed, size-exclusion chromatography, proteolytic mapping, optical spectroscopy, spin-label EPR,

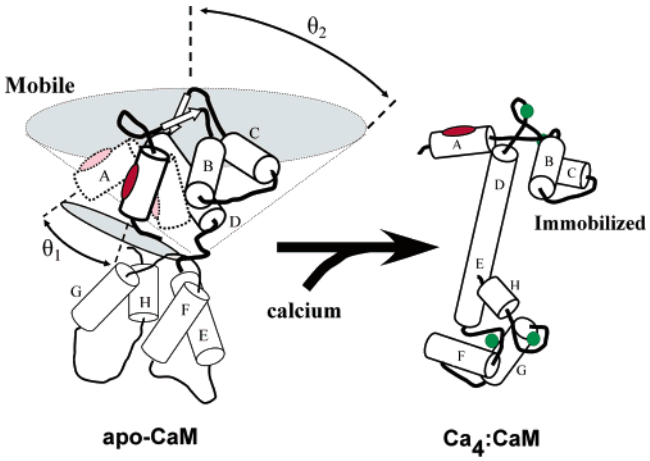

FIGURE 9: Model for calcium-dependent activation of CaM. FlAsH (red oval) bound to helix A is depicted to report the helical amplitude of motion with a cone angle $2\theta_1$ in apo-CaM. Calcium activation (green circles) rigidifies the structure of the amino-terminal domain of CaM, resulting in a stabilized binding pocket for target peptides and a structural coupling between helix A and both the amino- and carboxyl-terminal domains of CaM. Prior to calcium activation, helix A undergoes large amplitude motions ($\theta_1 = 15 \pm 3°$) relative to the amino-terminal domain with a correlation time of 1.1 ± 0.5 ns (Table 2). Amino-terminal domain elements, which are coupled to helix A, undergo independent motion relative to the carboxyl-terminal domain ($\theta_2 > 65°$) with a correlation time of 10 ± 1 ns. Following calcium activation, the structural coupling with helix A and the opposing domains facilitates the ordered association of the opposing domains with variable target proteins by stabilizing a binding cleft and minimizing interdomain interactions.

and NMR spectroscopy have demonstrated that the interdomain linker of CaM is metastable, mediating interdomain structural changes that modulate calcium affinity and target protein activation (*27*, *36*, *52*−*60*, *63*). The secondary structure of the interdomain linker is disrupted, with concomitant structural uncoupling of the opposing domains of CaM, under conditions of low salt, acidic pH, high temperature, or following site-directed mutagenesis of stabilizing interactions within helix H in the carboxyl-terminal domain (*27*, *45*−*47*, *55*). Thus, reported differences in the high-resolution structures of CaM are, in part, the result of differences in experimental conditions (*7*, *19*, *47*, *62*, *64*). In this respect, earlier results suggesting that calcium activation disrupts the helical structure of the central sequence connecting the opposing domains of CaM compared the structures of apo-CaM and calcium-activated CaM determined at 23 and 35 °C (*19*, *62*). Subsequent measurements demonstrated that the helical structure of the central sequence connecting the opposing domains of CaM essentially melts at temperatures above 35 °C (*47*). Thus, given the sensitivity of the structure of the central sequence to solution conditions and temperature, it is not surprising that there is greater order in the central sequence of apo-CaM at 23 °C in comparison to the calcium-bound state of CaM at 35 °C. Collectively, these results indicate that the average structures of CaM exist within a continuum of structures, and indicate a critical role for dynamic structural changes in mediating the different activities of CaM in response to calcium activation (*61*). Thus, CaM does not exist in a single well-defined structure; rather, helices have variable interhelical angles and are, at best, only approximately rigid (*20*).

Structural and Functional Coupling between Opposing Domains of CaM. At physiological ionic strengths and pH, the structural linkages between the occupancy of calcium binding sites located on the opposing globular domains of CaM are mediated through the stabilization of the central sequence located between Met^{76} and Ser^{81} (*52*, *57*, *59*). Thus, prior to calcium binding, there is conformational disorder in this sequence that is apparent using NMR, fluorescence, and spin-label EPR spectroscopy (*7*, *46*, *47*, *57*, *62*). Calcium binding stabilizes this sequence and strongly couples the opposing globular domains of CaM such that they undergo concerted rotational dynamics on the nanosecond time scale with an overall rotational correlation time of approximately 15 ± 2 ns (Table 2). This rate of motion is consistent with that expected for the overall concerted rotational motion of CaM calculated from hydrodynamic considerations for the structure shown in Figure 1 ($\varphi_r = 1/6D_r = 15.7$ ns) (*18*, *43*), and is in agreement with prior optical and NMR measurements (*46*, *47*). In contrast, independent rotational motion of the opposing domains is apparent at higher temperatures and acidic pH values, where the central helix essentially melts (*7*, *47*, *62*). These NMR measurements show that the central linker sequence transitions from a primarily helical structure at 35 °C to an essentially random coil at 43 °C (*47*). These latter NMR results are, moreover, consistent with observed increases in the conformational heterogeneity of the central linker sequence under acidic conditions (*46*), which emphasizes the dynamic instability of the calcium-activated structure of CaM associated with its ability to bind and activate target proteins with little sequence similarity. In this context, our current results suggest that the calcium-induced structural linkage between helix A and the central linker sequence functions as part of a conformational switch that stabilizes the activated conformation of CaM necessary for the productive binding and activation of more than 50 different target proteins.

Conclusions and Future Directions. In summary, prior to calcium activation, helix A undergoes large amplitude motions. Calcium binding induces helical rearrangements, which function to immobilize helix A through contact interactions with other helical elements in both the amino-terminal domain and the sequence between Lys^{77} and Asp^{95} that connects the opposing domains of CaM to induce a more ordered conformation with exposed binding clefts necessary for association with CaM-dependent target proteins (Figure 9).

REFERENCES

1. James, P., Vorherr, T., and Carafoli, E. (1995) Calmodulin-binding domains: Just two faced or multi-faceted? *Trends Biochem. Sci. 20*, 38−42.
2. Yap, K. L., Kim, J., Truong, K., Sherman, M., Yuan, T., and Ikura, M. (2000) Calmodulin target database, *J. Struct. Funct. Genomics 1*, 8−14.
3. Squier, T. C., and Bigelow, D. J. (2000) Protein oxidation and age-dependent alterations in calcium homeostasis, *Front. Biosci. 5*, 1−23.
4. Wang, H., and Storm, D. R. (2003) Calcium-regulated adenylyl cyclases: Cross-talk and plasticity in central nervous system, *Mol. Pharmacol. 63*, 463−468.
5. Fournier, V., Leclerc, P., Cormier, N., and Bailey, J. L. (2003) Implication of calmodulin-dependent phosphodiesterase type 1 during bovine sperm capacitation, *J. Androl. 24*, 104−112.
6. LaPorte, D. C., Wierman, B. M., and Storm, D. R. (1980) Calcium-induced exposure of a hydrophobic surface on calmodulin, *Biochemistry 19*, 3814−3819.

7. Chou, J. J., Li, S., Klee, C. B., and Bax, A. (2001) Solution structure of Ca^{2+}-calmodulin reveals flexible hand-like properties of its domains, *Nat. Struct. Biol. 8*, 990−997.
8. Goto, K., Toyama, A., Takeuchi, H., Takayama, K., Saito, T., Iwamoto, M., Yeh, J. Z., and Narahashi, T. (2004) Ca^{2+} binding sites in calmodulin and troponin C alter interhelical angle movements, *FEBS Lett. 561*, 51−57.
9. Yang, C., Jas, G. S., and Kuczera, K. (2004) Structure, dynamics and interaction with kinase targets: Computer simulations of calmodulin, *Biochim. Biophys. Acta 1697*, 289−300.
10. Persechini, A., McMillan, K., and Leaky, P. (1994) Activation of myosin light chain kinase and nitric oxide synthase activities by calmodulin fragments, *J. Biol. Chem. 23*, 16148−16154.
11. Crivici, A., and Ikura, M. (1995) Molecular and structural basis of target recognition by calmodulin, *Annu. Rev. Biophys. Biomol. Struct. 24*, 85−116.
12. Ehrhardt, M. R., Urbauer, J. L., and Wand, A. J. (1995) The energetics and dynamics of molecular recognition by calmodulin, *Biochemistry 34*, 2731−2738.
13. Sun, H., and Squier, T. C. (2000) Ordered and cooperative binding of opposing globular domains of calmodulin to the plasma membrane Ca-ATPase, *J. Biol. Chem. 275*, 1731−1738.
14. Kranz, J. K., Flynn, P. F., Fuentes, E. J., and Wand, A. J. (2002) Dissection of the pathway of molecular recognition by calmodulin, *Biochemistry 41*, 2599−2608.
15. Shifman, J. M., and Mayo, S. L. (2003) Exploring the origins of binding specificity through the computational redesign of calmodulin, *Proc. Natl. Acad. Sci. U.S.A. 100*, 13274−13279.
16. Yamniuk, A. P., and Vogel, H. J. (2004) Calmodulin's flexibility allows for promiscuity in its interactions with target proteins and peptides, *Mol. Biotechnol. 27*, 33−57.
17. Babu, Y. S., Bugg, C. E., and Cook, W. J. (1988) Structure of calmodulin refined at 2.2 Å resolution, *J. Mol. Biol. 204*, 191−204.
18. Chattopadhyaya, R., Mendor, W. E., Means, A. R., and Quiocho, F. A. (1992) Calmodulin structure refined at 1.7 Å resolution, *J. Mol. Biol. 228*, 1177−1192.
19. Kuboniwa, H., Tjandra, N., Grzesiek, S., Ren, H., Klee, C. B., and Bax, A. (1995) Solution structure of calcium-free calmodulin, *Nat. Struct. Biol. 2*, 768−776.
20. Wilson, M. A., and Brunger, A. T. (2000) The 1.0 Å crystal structure of Ca^{2+}-bound calmodulin: An analysis of disorder and implications for functionally relevant plasticity, *J. Mol. Biol. 301*, 1237−1256.
21. Jaren, O. R., Krantz, J. K., Sorensen, B. R., Wand, A. J., and Shea, M. A. (2002) Calcium-induced conformational switching of *Paramecium* calmodulin provides evidence for domain coupling, *Biochemistry 41*, 14158−14166.
22. Fallon, J. L., and Quiocho, F. A. (2003) A closed compact structure of native Ca^{2+}-calmodulin, *Structure 11*, 1303−1307.
23. Wriggers, W., Mehler, E., Pitici, F., Weinstein, H., and Schulten, K. (1998) Structure and dynamics of calmodulin in solution, *Biophys. J. 74*, 1622−1639.
24. Griffin, B. A., Adams, S. R., and Tsien, R. Y. (1998) Specific covalent labeling of recombinant protein molecules inside live cells, *Science 281*, 269−272.
25. Adams, S. R., Campbell, R. E., Gross, L. A., Martin, B. R., Walkup, G. K., Yao, Y., Liopis, J., and Tsien, R. Y. (2002) New biarsenical ligands are tetracysteine motifs for protein labeling in vitro and vivo: Synthesis and biological application, *J. Am. Chem. Soc. 124*, 6063−6075.
26. Strasburg, G. M., Hogan, M., Birmachu, W., Thomas, D. D., and Louis, C. F. (1988) Site-specific derivatives of wheat germ calmodulin. Interactions with troponin and sarcoplasmic reticulum, *J. Biol. Chem. 263*, 542−548.
27. Sun, H., Yin, D., Coffeen, L. A., Shea, M. A., and Squier, T. C. (2001) Mutation of Tyr^{138} disrupts the structural coupling between the opposing domains in vertebrate calmodulin, *Biochemistry 40*, 9605−9617.
28. Klee, C. B., Crouch, T. H., and Krinks, M. H. (1979) Calcineurin: A calcium- and calmodulin-binding protein of the nervous system, *Proc. Natl. Acad. Sci. U.S.A. 76*, 6270−6273.
29. Schiefer, S. (1986) Calmodulin, in *Methods of enzymatic analysis* (Bergmeyer, H. U., Bergmeyer, J., and Grable, M., Eds.) Vol. 9, pp 317−331, VCH Publishers, Deerfield Beach, FL.
30. Lakowicz, J. R. (1999) in *Principles of Fluorescence Spectroscopy*, 2nd ed., Kluwer Academic/Plenum Publishers, New York.
31. Gratton, E., and Limkeman, M. (1983) A continuously variable frequency cross-correlation phase fluorometer with picosecond resolution, *Biophys. J. 44*, 315−324.
32. Lakowicz, J. R., and Maliwal, B. (1985) Construction and performance of a variable-frequency phase-modulation fluorometer, *Biophys. Chem. 21*, 61−78.
33. Bevington, P. R. (1969) in *Data Reduction and Error Analysis for the Physical Sciences*, McGraw-Hill, New York.
34. Hunter, G. W., and Squier, T. C. (1998) Phospholipid acyl chain rotational dynamics are independent of headgroup structure in unilamellar vesicles containing binary mixtures of dioleoylphosphatidylcholine and dioleoyl-phosphatidylethanolamine, *Biochim. Biophys. Acta 1415*, 63−76.
35. Weber, G. (1981) Resolution of the fluorescence lifetimes in a heterogeneous system by phase and modulation measurements, *J. Phys. Chem. 85*, 949−953.
36. Faga, L. A., Sorensen, B. R., VanScyoc, W. S., and Shea, M. A. (2003) Basic interdomain boundary residues in calmodulin decrease calcium affinity of sites I and II by stabilizing helix−helix interactions, *Proteins 50*, 381−391.
37. Zhang, M., Li, M., Wang, J. H., and Vogel, H. J. (1994) The effect of Met → Leu mutations on calmodulin's ability to activate cyclic nucleotide phosphodiesterase, *J. Biol. Chem. 269*, 15546−15552.
38. Nakanishi, J., Maeda, M., and Umezawa, Y. (2004) A new protein conformation indicator based on biarsenical fluorescein with an extended benzoic acid moiety, *Anal. Sci. 20*, 273−278.
39. Chen, B., Jones, T. E., and Bigelow, D. J. (1999) The nucleotide-binding site of the sarcoplasmic reticulum Ca-ATPase is conformationally altered in aged skeletal muscle, *Biochemistry 38*, 14887−14896.
40. Chen, B., and Bigelow, D. J. (2002) Phosphorylation induces a conformational transition near the lipid-water interface of phospholamban reconstituted with the Ca-ATPase, *Biochemistry 41*, 13965−13972.
41. Steiner, R. E. (1991) in *Fluorescence Spectroscopy* (Lakowicz, J. R., Ed.) Vol. 2, pp 1−52, Plenum Press, New York.
42. Cantor, C. R., and Schimmel, P. R. (1980) *Biophysical Chemistry, Part II: Techniques for the study of biological structure and function*, p 461, W. H. Freeman and Co., San Francisco.
43. Garcia de la Torre, J., Huertas, M. L., and Carrasco, B. (2000) Calculation of hydrodynamic properties of globular proteins from their atomic-level structure, *Biophys. J. 78*, 719−730.
44. Small, E. W., and Anderson, S. R. (1988) Fluorescence anisotropy decay demonstrates calcium-dependent shape changes in photocross-linked calmodulin, *Biochemistry 27*, 419−428.
45. Yao, Y., Schöneich, C., and Squier, T. C. (1994) Resolution of structural changes associated with calcium activation of calmodulin using frequency domain fluorescence spectroscopy, *Biochemistry 33*, 7797−7810.
46. Sun, H., Yin, D., and Squier, T. C. (1999) Calcium-dependent structural coupling between opposing globular domains of calmodulin involves the central helix, *Biochemistry 38*, 12266−12279.
47. Chang, S.-L., Szabo, A., and Tjandra, N. (2003) Temperature dependence of domain motions of calmodulin probes by NMR relaxation at multiple fields, *J. Am. Chem. Soc. 125*, 11379−11384.
48. Beechem, J. M., Gratton, E., Ameloot, M., Knutson, J. R., and Brand, L. (1991) The global analysis of fluorescence intensity and anisotropy decay data: Second generation theory and programs, in *Topics in Fluorescence Spectroscopy* (Lakowicz, J. R., Ed.) pp 241−305, Plenum Press, New York.
49. Kinosita, K., Jr., Ishiwata, S., Yoshimura, H., Asai, H., and Ikegami, A. (1984) Submicrosecond and microsecond rotational motions of myosin head in solution and in myosin synthetic filaments as revealed by time-resolved optical anisotropy decay measurements, *Biochemistry 23*, 5963−5975.
50. Prochniewicz, E., Zhang, Q., Howard, E. C., and Thomas, D. D. (1996) Microsecond rotational dynamics of actin: Spectroscopic detection and theoretical simulation, *J. Mol. Biol. 255*, 446−457.
51. Sabbert, D., Engelbrecht, S., and Junge, W. (1997) Functional and idling rotatory motion within F1-ATPase, *Proc. Natl. Acad. Sci. U.S.A. 94*, 4401−4405.
52. Shea, M. A., Verhoeven, A. S., and Pedigo, S. (1996) Calcium-induced interactions of calmodulin domains revealed by quantitative thrombin footprinting of Arg37 and Arg106, *Biochemistry 35*, 2943−2957.
53. Yao, Y., Yin, D., Jas, G., Kuczera, K., Williams, T. D., Schöneich, Ch., and Squier, T. C. (1996) Oxidative modification of a carboxyl-terminal vicinal methionine in calmodulin by hydrogen

peroxide inhibits calmodulin-dependent activation of the plasma membrane Ca-ATPase, *Biochemistry 35*, 2767−2789.
54. Gao, J., Yin, D., Yao, Y., Sun, H., Qin, Z., Schöneich, Ch., Williams, T. D., and Squier, T. C. (1998) Loss of conformational stability in calmodulin upon methionine oxidation, *Biophys. J. 74*, 1115−1134.
55. Yin, D., Kuczera, K., and Squier, T. C. (2000) The sensitivity of carboxyl-terminal methionines in calmodulin isoforms to oxidation by H_2O_2 modulates the ability to activate the plasma membrane Ca-ATPase, *Chem. Res. Toxicol. 13*, 103−110.
56. Yin, D., Sun, H., Ferrington, D. A., and Squier, T. C. (2000) Closer proximity between opposing domains of vertebrate calmodulin following deletion of Met^{145}−Lys^{148}, *Biochemistry 39*, 10255−10268.
57. Qin, Z., and Squier, T. C. (2001) Calcium-dependent stabilization of the central sequence between Met76 and Ser81 in vertebrate calmodulin, *Biophys. J. 81*, 2908−2918.
58. VanScyoc, W. S., and Shea, M. A. (2001) Phenyalanine fluorescence studies of calcium binding to N-domain fragments of Paramecium calmodulin mutants show increased calcium affinity correlates with increased disorder, *Protein Sci. 10*, 1758−1768.
59. Sorensen, B. R., Faga, L. A., Hultman, R., and Shea, M. A. (2002) An interdomain linker increases the thermostability and decreases the calcium affinity of the calmodulin N-domain, *Biochemistry 41*, 15−20.
60. VanScyoc, W. S., Sorensen, B. R., Rusinova, E., Laws, W. R., Ross, J. B. A., and Shea, M. A. (2002) Calcium binding to calmodulin mutants monitored by domain-specific intrinsic phenyalanine and tyrosine fluorescence, *Biophys. J. 83*, 2767−2780.
61. Vigil, D., Gallagher, S. C., Trewhella, J., and Garcia, A. E. (2001) Functional dynamics of the hydrophobic cleft in the N-domain of calmodulin, *Biophys. J. 80*, 2082−2092.
62. Barbato, G., Ikura, M., Kay, L. E., Pastor, R. W., and Bax, A. (1992) Backbone dynamics of calmodulin studied by nitrogen-15 relaxation using inverse detected two-dimensional NMR spectroscopy: The central helix is flexible, *Biochemistry 31*, 5269−5278.
63. Gao, J., Yao, Y., and Squier, T. C. (2001) Oxidatively modified calmodulin binds to the plasma membrane Ca-ATPase in a nonproductive and conformationally disordered complex, *Biophys. J. 80*, 1791−1801.
64. Ikura, M., Spera, S., Barbato, G., Kay, L. E., Krinks, M., and Bax, A. (1991) Secondary structure and side-chain proton and carbon-13 resonance assignments of calmodulin in solution by heteronuclear multidimensional NMR spectroscopy, *Biochemistry 30*, 9216−9228.
65. Jencks, W. P. (1969) *Catalysis in Chemistry and Enzymology*, pp 564−565, McGraw-Hill, New York.

BI048332U